# Hydration Water and Swelling Behavior of Magadiite. The H+, Na+, K+, Mg2+, and Ca2+ Exchanged Forms

**ARTICLE** *in* THE JOURNAL OF PHYSICAL CHEMISTRY B · JANUARY 2002

Impact Factor: 3.3 · DOI: 10.1021/jp012981n

# Hydration Water and Swelling Behavior of Magadiite. The $H^+$, $Na^+$, $K^+$, $Mg^{2+}$, and $Ca^{2+}$ Exchanged Forms

**Céline Eypert-Blaison,*,† Laurent J. Michot,*,† Bernard Humbert,‡ Manuel Pelletier,† Frédéric Villiéras,† and Jean-Baptiste d'Espinose de la Caillerie§**

*Laboratoire Environnement et Minéralurgie, INPL-ENSG-CNRS UMR 7569, BP 40, 54501 Vandoeuvre Cedex, France, Laboratoire de Chimie Physique Pour l'Environnement, UMR CNRS-UHP, Nancy I 7564, 54600 Villers-los-Nancy, France, and Laboratoire de Physique Quantique, CNRS FRE 2312, Ecole Supérieure de Physique et de Chimie Industrielles, 10 rue Vauquelin, 75231 Paris Cedex 05, France*

*Received: August 2, 2001; In Final Form: November 13, 2001*

The hydration behavior of synthetic magadiite exchanged with $H^+$, $Na^+$, $K^+$, $Mg^{2+}$, and $Ca^{2+}$ was investigated by combining thermal analyses, water adsorption gravimetry, X-ray diffraction, and spectroscopic techniques, including $^{29}Si$ NMR, infrared, and Raman under various pressures. Thermal analyses reveal distinct water populations, the number of which depends on the valency of the cation. Except for H-magadiite, which does not swell, water adsorption isotherms exhibit two steps, corresponding to two increases of the interlayer distance. These phenomena are shifted toward higher relative pressures in the case of divalent exchanged samples. For Na- and K-magadiite, the adsorption of the first water molecules generates a water molecule in a $C_1$ symmetry, interacting simultaneously with both the cation and the surface. For higher relative pressure, two new populations of water molecules appear: (i) water molecules linked to the cation and (ii) doubly hydrogen-bonded molecules. In the case of $Mg^{2+}$, the first hydration step is much less clearly defined and spectroscopic analyses suggest the simultaneous existence of water molecules in $C_1$ symmetry and linked to the magnesium cations. Finally, when calcium ions are exchanged in the interlayer space, they interact strongly with $SiO^-$ groups and water/cation interactions are not strong enough for displacing $Ca^{2+}$ from its initial position. For this reason, no water molecules in $C_1$ symmetry develop and only water molecules linked to the cation are observed at first. For higher relative pressures, liquidlike water molecules are present in the intragallery space but no doubly hydrogen-bonded network develops.

## Introduction

Solids with layered structures possess basal planes of atoms that are tightly bonded within the planes but relatively weakly bonded in the direction perpendicular to the planes. In several classes of layered solids, such as smectite clay minerals, layered double hydroxides, group 4 metal phosphates, calcium silicate hydrates, or layered silicic acids, the solid layers carry a net electrical charge. This electrical charge is compensated by counterions occupying the gallery region between layers. Because of the presence of these charge-balancing ions, the interlayer space is generally accessible to water molecules, which can then provoke a swelling of the structure in the direction perpendicular to the layers. Consequently, the status and location of water molecules in the intergallery space and its evolution with water vapor relative pressure largely control the mechanical strength, ionic conductivity, acid−base properties, and ion-exchange behavior of charged layered solids.

Because of their ubiquituous presence in soils, the most extensively studied family of charged layered solids is by far swelling clay minerals. Numerous experimental works[1] and computer simulation studies[2] have been devoted to understanding the arrangement of water molecules in the interlayer spaces of clay minerals and its evolution with increasing water content. It appears clearly, especially for low-charged materials, that cation hydration plays a major role in controlling the initial swelling stages. For higher charges, there is still an ongoing debate regarding the relative importance of water/cation and water/surface interactions. Comparatively, very little is known on the detailed hydration behavior of other classes of charged layered solids, except for a few studies.[3−7] This appears rather surprising because such information could shed new light on the role of charge amount, charge localization, and layer structure on the arrangement of water molecules in confined interlayer spaces.

For this reason, we recently focused our attention on magadiite, the most studied member of the family of hydrous sodium silicates. Magadiite was first found and described by Eugster who reported its chemical composition as $Na_2Si_{14}O_{29}\cdot 9H_2O$.[8] Because of the small dimensions of single crystals of natural and synthetic magadiite, the exact structure of this mineral remains unknown. Still, it is clear that Na-magadiite is a charged layered structure in which solid layers are formed by the arrangement of silicon tetrahedra that contain terminal oxygen atoms neutralized by intragallery $Na^+$ ions. As shown by McAtee et al.[9] and Brindley,[10] the interlamellar distance of Na-magadiite evolves with water content, thus revealing a swelling character. Though various studies mention the importance of water content on the structure of this mineral,[11−13] the swelling pathway of Na-magadiite and the status of water molecules with increasing water content was not fully known

* To whom correspondence should be addressed. E-mail for C.E.-B.: celine.eypert-blaison@inrs.fr. E-mail for L.J.M.: laurent.michot@ensg.inpl-nancy.fr.

† Laboratoire Environnement et Minéralurgie.

‡ Laboratoire de Chimie Physique pour l'Environnement.

§ Laboratoire de Physique Quantique.

10.1021/jp012981n CCC: $22.00 
Published on Web 12/14/2001

until recently. In a previous paper, we analyzed this phenomenon in detail by combining thermal analyses, water adsorption gravimetry, and X-ray diffraction and infrared spectroscopy under controlled water pressure.[14] Such a study clearly evidenced three distinct hydrated states for Na-magadiite. In addition, it also revealed that cation hydration alone does not explain water adsorption in this mineral and that water/cation/surface interactions play a major role as well in structuring water molecules. Furthermore, by comparing Na-magadiite and its proton-exchanged form, H-magadiite, and by focusing on the evolution of the vibrational spectra of the silicate layers, we were able to refine the three different statuses of water molecules on the basis of evolving cation/water/layer interaction.[15] The aim of the present paper is to apply the same approach to various ion-exchanged forms of magadiite by studying in parallel, upon water adsorption, the structural changes of water molecules as well as the possible modifications of the silicate layer. We will show that, depending on the nature of the interlayer cation, the delicate balance of the various interactions between water, cation, and solid layers can lead to distinct swelling behaviors.

## Experimental Section

**Materials.** Na-magadiite was synthesized according to the procedure described by Fletcher et al.[16] The crystallinity and purity were checked by powder X-ray diffraction measurements (Jobin-Yvon Sigma 2080 diffractometer). According to chemical and thermal analyses, the unit cell formula of Na-magadiite can be written as $Na_{2.07}H_{1.93}Si_{14}O_{30}\cdot 8.27H_2O$. [14,15] On the basis of this formula and assuming that all sodium cations are exchangeable, the resulting theoretical cationic exchange capacity would be equal to 225 mequiv/100 g. In addition, the theoretical surface area of this sample is around 710 $m^2\ g^{-1}$.

The H-magadiite form was obtained from a slow potentiometric titration of Na-magadiite with aqueous HCl.[17] The final product was air-dried. Its unit cell formula can be written as $H_4Si_{14}O_{30}\cdot 0.5H_2O$. The K-, Mg-, and Ca− forms were obtained by suspending twice the starting Na-magadiite in a 0.1 M KCl, $MgCl_2$, and $CaCl_2$ solution, respectively. To avoid undesirable proton exchange, solutions were stabilized at pH = 9 with KOH, $Mg(OH)_2$, and $Ca(OH)_2$, respectively. The resulting suspensions were then washed until chloride-free and air-dried. The purity and crystallinity were checked by powder X-ray diffraction measurements (Jobin-Yvon Sigma 2080 diffractometer), whereas the absence of precipitated carbonates or hydroxides was verified by IR measurements (Bruker IFS 55 Fourier transform spectrometer). According to chemical and thermal analyses, unit cell formulas of K-magadiite, Mg-magadiite, and Ca-magadiite can be written as $K_{1.86}H_{2.14}Si_{14}O_{30}\cdot 8.04H_2O$, $Mg_{0.96}H_{2.08}Si_{14}O_{30}\cdot 4.15H_2O$, and $Ca_{0.97}H_{2.06}Si_{14}O_{30}\cdot 5.77H_2O$, respectively.

**Methods.** Nitrogen adsorption−desorption isotherms at 77 K were obtained using a lab-built classical step-by-step volumetric setup. Prior to the experiments, the samples were outgassed at 50 °C under a residual pressure of 0.1 Pa during 18 h. Surface area was determined using the BET treatment.

Controlled-transformation-rate thermal analysis (CTRTA), described by Rouquerol,[18] is coupled with a quadrupole mass spectrometer. In this process, the heating rate is not fixed but directly depends on the gas pressure generated by outgassing or reactions occurring during sample heating. The experimental conditions selected in the present study were a sample mass of 235 mg, a residual pressure of 2 Pa, and a heating rate of 1 °C/min from −196 to 400 °C. Between −196 °C and 20 °C, the increase in temperature is not controlled by pressure and corresponds to the free heating of the sample at a rate of ∼0.5 °C/min. From 20 °C upward, true CTRTA conditions are used with a maximal heating rate of 2 °C/min. The apparatus is coupled with a mass spectrometer to identify and quantify gas emission. The mass spectra were obtained on a Balzers QMG 420C mass spectrometer.

The MAS NMR $^{29}Si$ spectra were recorded on a Bruker MSL 300 spectrometer at 59.62 MHz. Hydrated samples were placed into 7 mm rotors and spun at 2 kHz. One-pulse $^{29}Si$ spectra were recorded using a pulse width ($\pi/2$) of 3.9 $\mu$s. The recycle delay was 3s, and 400 transients were accumulated. $\{^1H-^{29}Si\}$ CP/MAS NMR spectra were obtained with $\pi/2$ proton pulses of 5 $\mu$s, contact times of 6 ms, recycle delays of 5 s, and 10 000 transients. The chemical shifts were quoted relative to tetramethylsilane.

Water vapor gravimetric adsorption experiments were carried out using a lab-built quasi-equilibrium setup designed around a Setaram MTB 10-8 symmetrical microbalance. Water vapor was supplied to the sample (thermostated at 30 °C) from a source kept at 41 °C at a slow flow rate to ensure quasi-equilibrium conditions at all times. The simultaneous recording of mass uptake and equilibrium pressure directly yields the water vapor adsorption isotherm. The experimental conditions were a sample mass of 105 mg and an outgassing at 50 °C during 18 h under a residual pressure of 1 Pa.

The evolution of X-ray diffraction patterns with water relative pressure was followed using a specially designed experimental setup. The oriented sample was placed inside a chamber allowing the control of relative humidity and temperature. The chamber kept at 30 °C is connected to a water vapor source. The water relative pressure in the chamber is controlled by changing the temperature of the source. X-ray diffraction patterns are recorded simultaneously over 30° ($\theta$) on an Inel CPS 120 curved detector using transmission geometry with Co K$\alpha$ radiation. The sample is outgassed before the experiment at 50 °C under a residual pressure of $10^{-3}$ Torr during 24 h. For each hydration state, the X-ray diffraction patterns were recorded after 24 h of equilibrium time.

IR spectra were recorded using an IR transmission cell specially designed for investigating the first hydration states of clay minerals.[19] The temperature and moisture of the sample are controlled. For these experiments, a magadiite film was prepared by depositing a few drops of a dilute aqueous suspension onto a ZnSe slide. The film is kept at 30 ± 0.1 °C. The relative water vapor pressure is controlled in the cell in a $P/P_0$ range between 0.01 and 0.85 by setting the temperature of a water source between −29 and +27.2 ± 0.1 °C. The cell is equipped with ZnSe windows. The FT-IR spectra were recorded on a Bruker FT-IR spectrometer using a DTGS detector. The IR spectra consisted of 100 averaged scans in the range of 7000−400 $cm^{-1}$ with a resolution of 2 $cm^{-1}$. The spectra were recorded at least 24 h after changing the temperature of the water vapor source.

The Raman spectra excited by the laser beam of an argon Spectra Physic Laser Stabilité 2017 were collected on a Jobin-Yvon T64000 spectrometer equipped with an optical microscope, a threefold monochromator, and a charged coupled camera (CCD) cooled at 144 K. The laser beam at the 514.5 nm wavelength was focused using a long frontal ×50 objective (numerical aperture = 0.5) on an area of about 3 $\mu m^2$. Ambient-condition experiments at 25 °C ± 2 °C were carried out using a laser power on the sample of approximately 30 mW. Vacuum experiments were performed in a closed cell, related to a primary vacuum up to $10^{-2}$ mbar, with a laser power of approximately 45 mW on the sample. The backscattered Raman spectra were

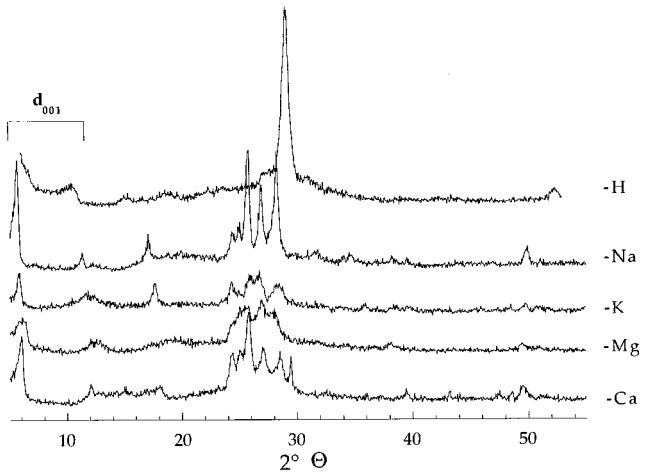


**Figure 1.** X-ray powder diffraction pattern of the five exchanged magadiites.

**TABLE 1: Basal Distances, $d_{001}$ (Å), for the Five Ion-Exchanged Magadiites and Their Coherent Scattering Thickness, $D$ (Å)**

| | $d_{001}$ (Å) | $D$ (Å) |
|---|---|---|
| H-magadiite | 11.8 | 65 |
| Na-magadiite | 15.5 | 262 |
| K-magadiite | 14.9 | 179 |
| Mg-magadiite | 14.7 | 79 |
| Ca-magadiite | 14.7 | 135 |

collected in a confocal mode to avoid optical artifact. The spectral resolution was 3 $cm^{-1}$ with a wavenumber precision better than 1 $cm^{-1}$.

## Results and Discussion

**Characterization of the Starting Ion-Exchanged Magadiite Samples.** To check that ion exchange does not provoke any major structural changes and that the basic layered structure of the material is conserved, X-ray diffraction patterns and $^{29}Si$ MAS NMR spectra were measured for the five ion-exchanged magadiite samples. Though changes can be observed on the diffractograms (Figure 1), two arguments show that the layered structure of the initial Na-magadiite is conserved after cation exchange: (i) As shown in Table 1, most of the observed variations related to the nature of the interlayer cation can indeed be assigned to changes in the number of stacked elementary layers (around 5 for H- and Mg-magadiites, 9 for Ca-magadiite, 12 for K-magadiite, and 17 for Na-magadiite). (ii) $^{29}Si$ MAS NMR spectra of the five samples (Figure 2) display only signals assignable to silicon atoms in $Q^3$ or $Q^4$ coordination. The $Q^3/Q^4$ ratio (Table 2) is equal to 0.4 for all of the studied samples, which reveals that the number of silicon tetrahedra and their arrangement in the layers are not strongly modified upon cation exchange. Except for K-magadiite, which exhibits an upfield shoulder, only one $Q^3$ signal is observed. The chemical shift of $Q^3$ depends on the nature of the interlayer cation (Table 2), which strongly suggests that cations are located in the vicinity of the $Si-O^-$ groups. The fact that the NMR spectra do not exhibit two distinct $Q^3$ signals corresponding to $Si-O^-$ and Si−OH is likely due to the relatively high amount of water in the samples. Indeed, high humidity likely allows fast exchanges between the two species, which, in turn, yield a single average resonance. Three distinct $Q^4$ signals can be seen in the spectra corresponding to Na- and K-magadiite, whereas H-, Mg-, and Ca-magadiite exhibit a broad massive with a downfield shoulder. Still, the nature of the exchangeable cation does not appear to provoke any displacement of the $Q^4$ signals. The influence of the nature of the cation on the $Q^4$ peaks is then mainly revealed through a broadening of the signals, divalent species, and proton leading to broader signals. Such a tendency observed for ilerite samples[20] can be assigned to a broader distribution of chemical shifts resulting from an ordering loss in the structural network. Magadiite exchanged with divalent cations then presents a broader distribution of Si−O−Si angles. When the same samples are analyzed using the cross-polarization technique (Figure 3), the relative intensity of $Q^3$ signals clearly increases without any changes in position compared to classical MAS experiments (Table 2), which reveals that protons are closer to silicon atoms in $Q^3$ coordination than to those in $Q^4$ positions. CP-MAS experiments also result in a better discrimination of the $Q^4$ signals for H- and Mg-magadiite because three distinct peaks can then be observed.

The characterization results obtained for the five different ion-exchanged forms of magadiite clearly reveal common features for all of the samples, that is, a layered structure with a constant amount of $Q^3$ and $Q^4$ environments. The nature of the exchangeable cations appears to influence the stacking of elementary layers, which clearly depends on the polarizability of the interlayer species. Other changes related to the valency of the cation can be deduced from the $^{29}Si$ NMR spectra and reveal several chemical environments of Si atoms for divalent interlamellar cations.

**Role of the Exchangeable Cation on Water Adsorption Features.** *Thermal Analysis.* As shown in various studies dealing with water-swellable materials,[1h,1i,14] controlled transformation rate thermal analysis (CTRTA) is well-adapted to discriminate between various families of adsorbed water molecules. Figure 4 presents for the five magadiite samples the derivative curves of weight loss calculated from the intensity of the mass 18 analyzed by mass spectrometry. The corresponding weight losses are equal to 1.8%, 13.5%, 13.2%, 9.4%, and 6.8% for H-, Na-, K-, Mg-, and Ca-magadiite, respectively. Three groups can then be clearly distinguished: H-magadiite with a very low weight loss, divalent-exchanged samples with medium weight losses, and monovalent-exchanged magadiites with higher weight losses. In the first case (Figure 4a), only one single peak centered around −4 °C can be observed. In the second case (Figures 4d and 4e), two peaks located at −24 and 1 °C (Mg-magadiite) and −19 and 14 °C (Ca-magadiite) can be distinguished. Finally, for monovalent-exchanged samples, one observes three distinct peaks located at −14, 15, and 25 °C for the Na form and at −29, −11, and 5 °C for the K sample. CTRTA results then clearly suggest the existence of various water statuses for the different exchanged forms of magadiite, the number of which depends on the valency of the cation for swellable materials. Indeed, the low water content and single peak observed for H-magadiite can be related to the fact that such a sample does not adsorb water molecules in the interlayer space.[15,21,22]

*Water Adsorption Gravimetry and X-ray Diffraction under Controlled Water Pressure.* The water adsorption−desorption isotherms obtained at 303 K for the five magadiite samples are presented in Figure 5. As already suggested by CTRTA results (Figure 4), water uptake by H-magadiite remains very limited on the whole range of water relative pressure, especially when compared to the other ion-exchanged materials. This feature is particularly well illustrated in Table 3, which presents together the specific surface areas obtained for the five different samples using either nitrogen or water as an adsorbate. Even if the notion of specific surface area could be debatable in the case of swelling materials,[23] data from Table 3 clearly show that, except for

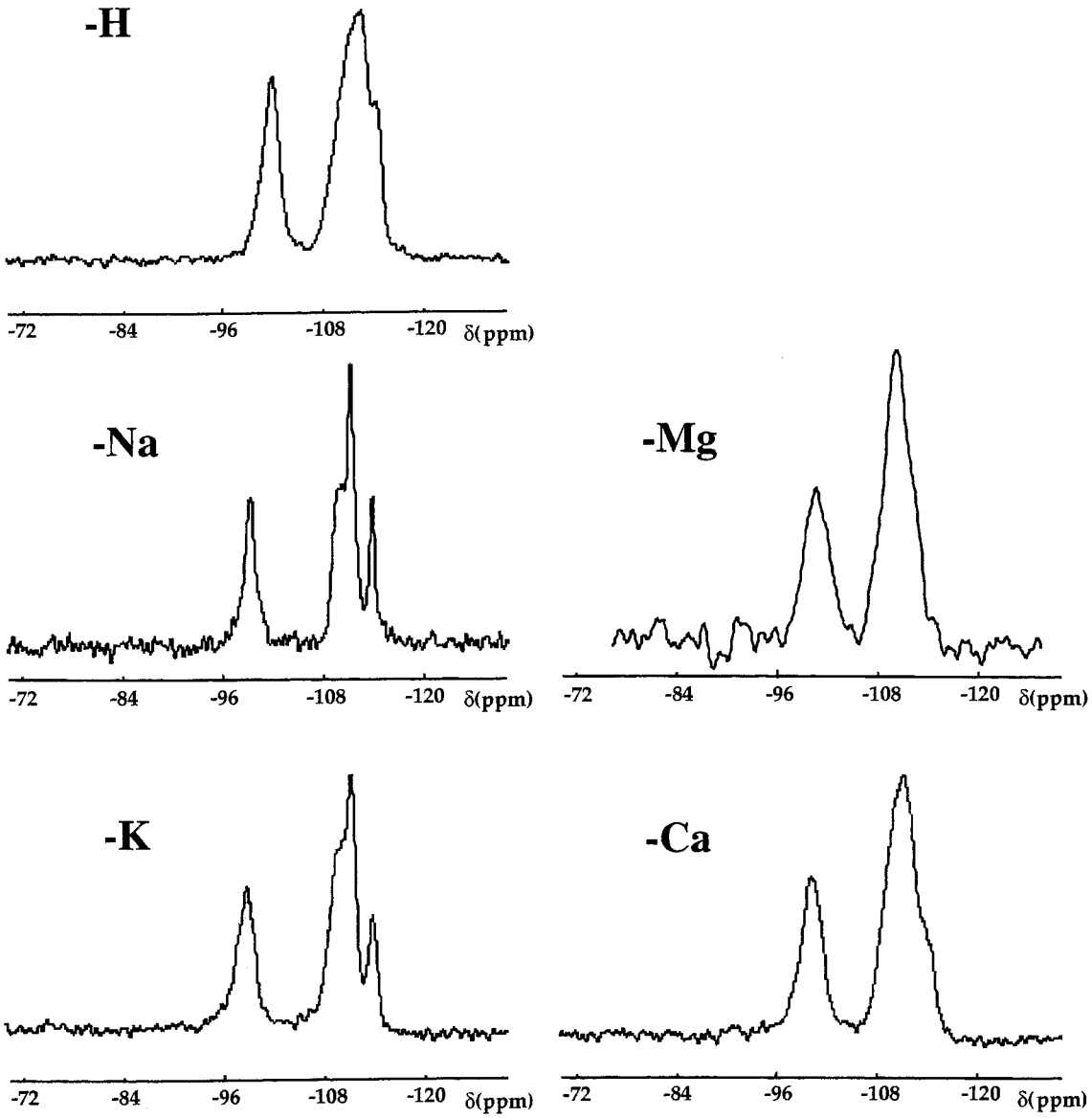


**Figure 2.** $^{29}$Si MAS NMR spectra of the five ion-exchanged magadiites. All chemical shifts values are given in ppm from liquid $Me_4Si$.

H-magadiite, the water BET surface area is much higher than the corresponding nitrogen one. The presence of a hysteresis loop extending down to low water pressures in desorption could be interpreted as indicative of the presence of micropores in the sample. However, we recently showed[14] that, in the case of Na-magadiite, water uptake and release were governed by the same mechanisms. The hysteresis loops can then be assumed to be related to different activation energies in adsorption or desorption.

As already suggested by CTRTA results, the shape of the isotherms is strongly affected by the valency of the interlayer cation, Na and K samples exhibiting similar shapes, as well as Mg- and Ca-magadiites. The isotherms corresponding to monovalent samples display two well-defined steps for $P/P_0$ values of around 0.05 and 0.12. In the case of divalent samples, the curves are much less resolved. A first step can be observed around $P/P_0$ values of 0.2 and 0.25 for Ca- and Mg-magadiites, respectively. A small inflection can also be noticed for $P/P_0$ values around 0.4 for Ca-magadiite and 0.5 for Mg-magadiite. Such a behavior is opposite to that observed for montmorillonite clay samples in which water adsorption isotherms exhibit a sharper rise for increasing polarizing power of the interlayer cation. In the case of montmorillonite, hydration was shown to be mainly governed by cation−water interactions.[1] The features observed for magadiite samples strongly suggest that for such materials layer/cation/water interactions also play a determining

**TABLE 2: $^{29}$Si MAS and CP-MAS NMR Chemical Shifts (ppm) and Calculated $Q^3/Q^4$ Ratios for the Five Ion-Exchanged Magadiites**

| | MAS | | CP-MAS | | |
|---|---|---|---|---|---|
| | $Q^3$ | $Q^4$ | $Q^3$ | $Q^4$ | Ratio $Q^3/Q^4$ |
| H-magadiite | −101.7 | −111.7 | −101.7 | −109.0 | 0.4 |
| | | −114.5 | | −111.5 | |
| | | | | −114.1 | |
| Na-magadiite | −99.1 | −109.6 | −99.1 | −109.7 | 0.4 |
| | | −111.1 | | −111.1 | |
| | | −113.7 | | −113.7 | |
| K-magadiite | −97.5 | −109.7 | −97.6 | −109.7 | 0.4 |
| | −98.7 | −111.3 | −98.8 | −111.4 | |
| | | −113.8 | | −113.9 | |
| Mg-magadiite | −99.7 | −111.5 | −100.6 | −108.4 | 0.4 |
| | | −113.7 | | −111.4 | |
| | | | | −114.0 | |
| Ca-magadiite | −100.0 | −110.7 | −100.7 | −110.6 | 0.4 |
| | | −114.0 | | −114.2 | |

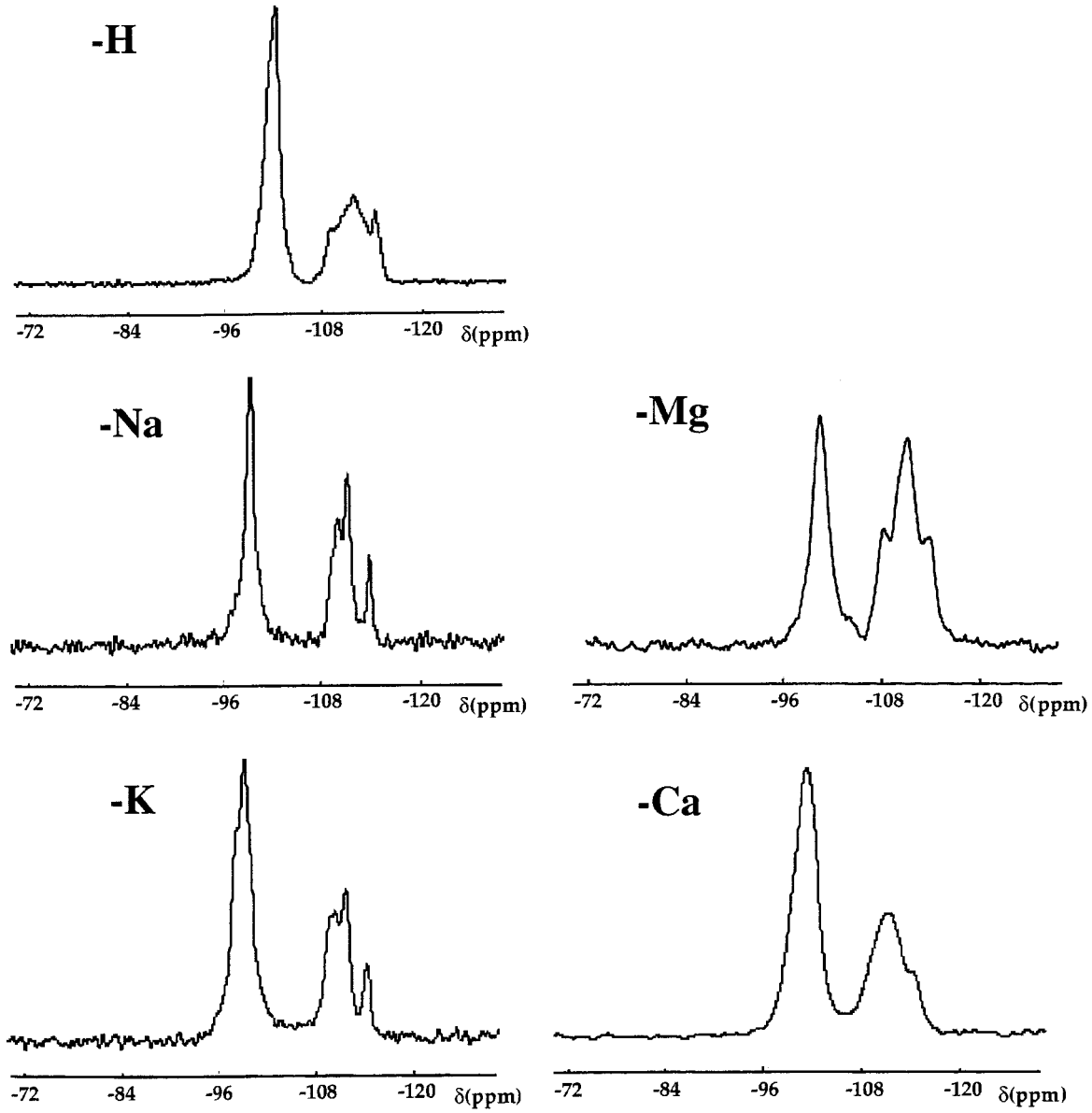


**Figure 3.** $^{29}$Si CP-MAS NMR spectra of the five ion-exchanged magadiites. All chemical shifts values are given in ppm from liquid $Me_4Si$.

role in controlling hydration behavior. To probe the structural changes occurring along the water adsorption isotherms, the evolution of the basal distance, $d_{(001)}$, with water pressure was plotted for the four swelling samples (Figure 6). Under vacuum, for both monovalent and divalent samples, the interlayer distance is directly linked to the size of the exchangeable cation as it evolves from 12.3 to 12.7 Å between $Na^+$ (ionic radius, 0.95 Å) and $K^+$ (ionic radius, 1.33 Å) and from 13.3 to 13.6 Å between $Mg^{2+}$ (ionic radius, 0.65 Å) and $Ca^{2+}$ (ionic radius, 0.99 Å). However, the origin for the differences between monovalent and divalent cations cannot be explained on the basis of size and must then be related somehow to the arrangement of cations with regard to the silica framework. The evolution of $d(001)$ with water pressure reproduces the various steps described on the water adsorption isotherms (Figure 5). The steps observed in the case of Na- and K-magadiites are accompanied by sharp increases of the basal distance, whereas the evolution of $d(001)$ for divalent-exchanged samples exhibits much less steep changes in agreement with the adsorption isotherms. The small inflections observed on the adsorption isotherms of Ca- and Mg-magadiite around $P/P_0 = 0.5$ appear to be related to changes in the interlamellar distances. As already shown for Na-magadiite,[14] these steps cannot be assigned to the development of successive layers of water molecules as the increase in interlamellar distance is always much lower than 3 Å.

*Infrared Spectroscopy Study of Water Signals.* As shown in numerous studies dealing with the hydration of swelling minerals,[23−25] infrared spectroscopy can provide detailed information about water structure in interlayer spaces. We then followed the evolution of the infrared spectra of the different ion-exchanged forms of magadiite with water adsorption. Spectra obtained upon water desorption (not shown) provide similar information in agreement with water adsorption gravimetry and XRD results, which evidenced reversible hydration phenomena. Figure 7 presents the evolution with water relative pressure of the spectra of H-magadiite in the regions corresponding to water bending (Figure 7A) and water stretching vibrations (Figure 7B). The spectra exhibit very few changes. In the bending region, a single band at 1627 $cm^{-1}$ displays a weak increase with water adsorption. In the stretching domain, only the signal around 3400 $cm^{-1}$ evolves with water pressure. In contrast, all of the signals corresponding to Si−OH groups with very little H bonding (3624 and 3584 $cm^{-1}$) remain

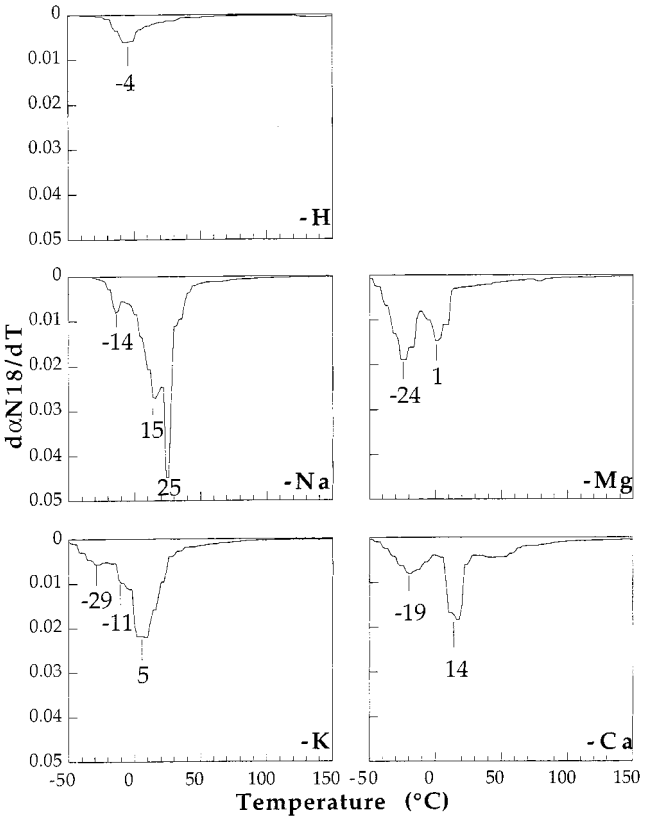


**Figure 4.** Derivative curves obtained from CTRTA experiments, for mass 18, for the five ion-exchanged magadiites.

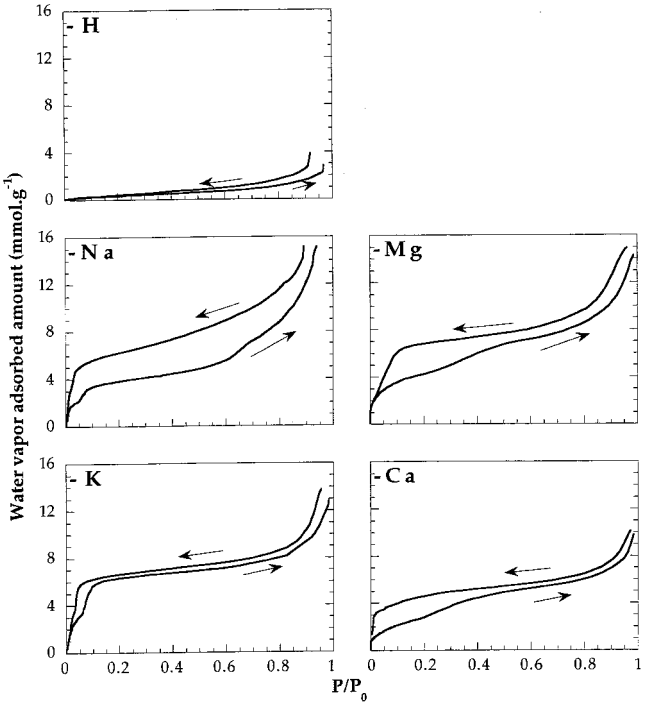


**Figure 5.** Water vapor adsorption−desorption isotherms at 30 °C onto the five ion-exchanged magadiites.

unaffected by water content. The observed changes can be assigned to physisorbed water molecules on the external surfaces of the particles, which confirms the nonswelling character of H-magadiite.

The infrared spectra obtained for Na- and K-magadiite under increasing water relative pressure are shown in Figure 8. In the bending region (Figure 8A,B), common features can be observed

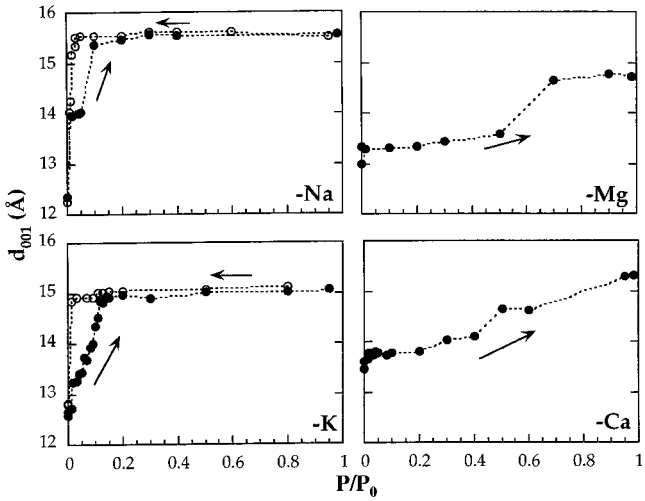


**Figure 6.** Evolution of the experimental 001 reflection of the four swelling ion-exchanged magadiites with water relative pressure at 30 °C.

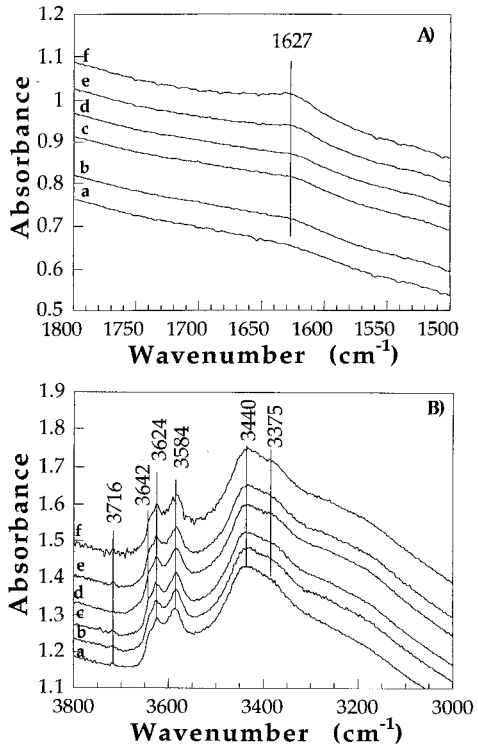


**Figure 7.** Evolution of infrared spectra of H-magadiite at 30 °C upon water adsorption in the water bending (A) and in the water stretching (B) vibration domains. For spectra a−f, conditions were under vacuum and $P/P_0 = 0.030$, 0.063, 0.100, 0.260, and 0.800.

**TABLE 3: BET Specific Surface Areas ($m^2/g$) of the Five Ion-Exchanged Magadiites, Using Nitrogen and Water as an Adsorbate**

| | ss $N_2$ ($m^2\ g^{-1}$) | ss $H_2O$ ($m^2\ g^{-1}$) |
|---|---|---|
| H-magadiite | 45 | 24 |
| Na-magadiite | 14 | 267 |
| K-magadiite | 27 | 390 |
| Mg-magadiite | 40 | 219 |
| Ca-magadiite | 30 | 323 |

for both samples, the tendencies being more marked for the Na-form. For low $P/P_0$, that is, in the first opening step evidenced by the evolution of $d(001)$ with water vapor pressure, a single band at 1635 $cm^{-1}$ is observed. It is much broader for K-magadiite (fwhh ≈ 70 $cm^{-1}$) than for the Na form (fwhh ≈

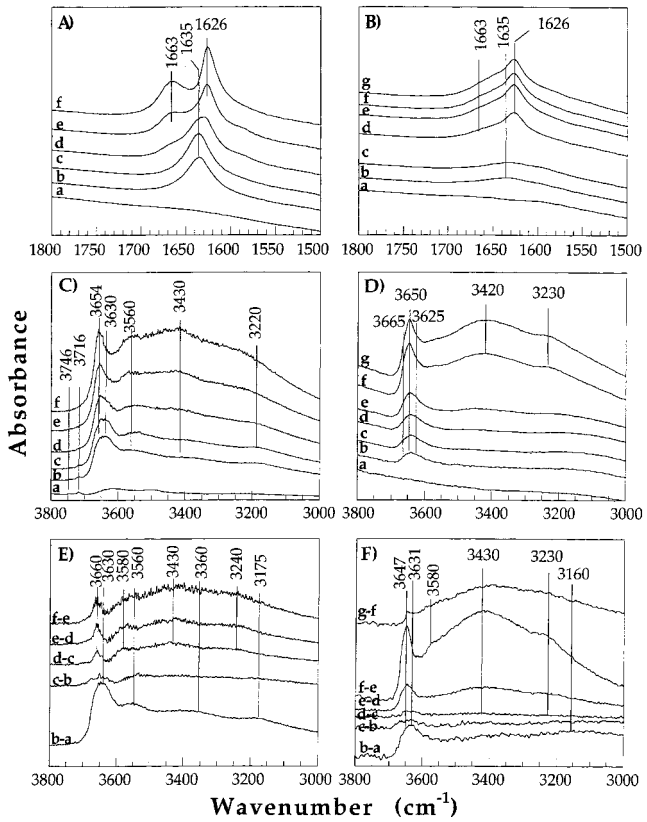


**Figure 8.** Evolution of infrared spectra at 30 °C upon water adsorption of Na-magadiite (A) and K-magadiite (B) in the water bending and in the water stretching (Na form, C; K form, D) vibration domains. In the case of Na-magadiite, conditions for spectra a−f were under vacuum and $P/P_0$ = 0.015, 0.040, 0.060, 0.080, and 0.600. In the case of K-magadiite, conditions for spectra a−g were under vacuum and $P/P_0$ = 0.015, 0.033, 0.050, 0.100, 0.400, and 0.600. Spectrum-to-spectrum subtraction of infrared signals in the water stretching vibrations for Na-magadiite (E) and K-magadiite (F) conditioned under various water vapor relative pressure are also shown.

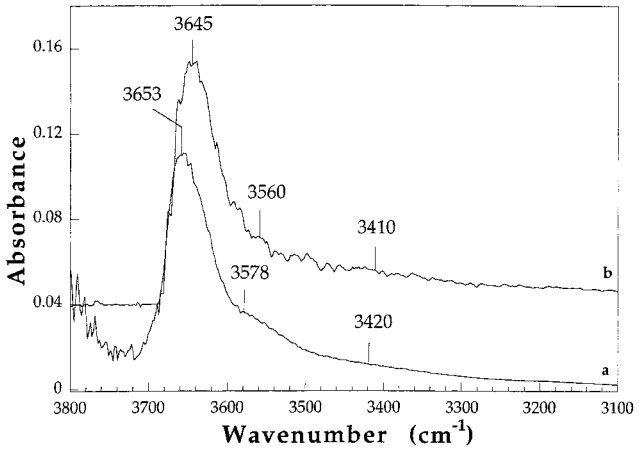


**Figure 9.** Corrected subtracted infrared spectra of (a) Na-magadiite and (b) K-magadiite.

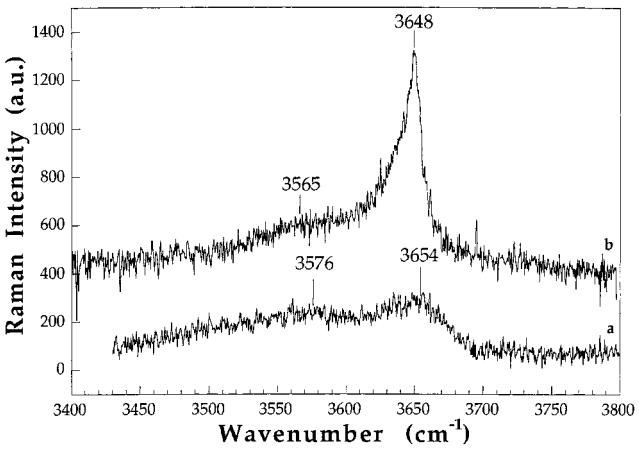


**Figure 10.** Raman spectra (3400−3800 cm$^{-1}$) at 25 °C of (a) Na-magadiite and (b) K-magadiite after short-time rehydration.

35 cm$^{-1}$). In the second opening step, the maximum of the $\nu_2$ band shifts toward lower wavenumbers at 1626 cm$^{-1}$ and a shoulder appears around 1663 cm$^{-1}$. The shape of the band at 1626 cm$^{-1}$ suggests that the initial component at 1635 cm$^{-1}$ may still be present. For higher relative pressures, the three components can be noticed with two distinct maxima at 1626 and 1663 cm$^{-1}$. The position at 1626 cm$^{-1}$ can be assigned to water molecules interacting with the monovalent cation and corresponds to the frequency observed in swelling clay minerals[1a−1e]. The signal at 1663 cm$^{-1}$ characterizes doubly hydrogen-bonded water molecules.[14] The position of the initial bending signal (1635 cm$^{-1}$) is similar to that observed in liquid water.[26] However, with regard to the important structural changes associated with the appearance of such a signal, it seems unlikely that this band can be assigned to liquid water. Another interpretation could be to relate the position of this component to what is observed in some binary water/organic bases 1:1 complexes in which $\delta$ $H_2O$ around 1630 cm$^{-1}$ can be obtained. According to such an assignment, the initial water molecules would be in a $C_1$ symmetry with two nonequivalent OH vibrations and would share interactions with both the cation and the silica framework.

Confirmation of this latter hypothesis should be obtained in the OH stretching region through the simultaneous appearance of both a low- and high-frequency signal. To better visualize changes in this range, both the raw spectra (Figure 8C,D) and the spectrum-to-spectrum subtraction have been plotted (Figure 8E,F). Under vacuum, the IR spectrum of Na-magadiite displays two weak signals around 3615 and 3490 cm$^{-1}$ that could be assigned to traces of hydration water. Such a feature can be related to CTRTA results, which show that at 30 °C under vacuum, Na-magadiite may not be fully dehydrated. Another interpretation could be to assign those two signals to the stretching of silanols. Between vacuum and $P/P_0$ = 0.015 (Figure 8E), new signals appear around 3630, 3560, 3360, and 3175 cm$^{-1}$ for Na-magadiite and around 3630, 3430, and 3160 cm$^{-1}$ for K-magadiite. In this spectral region, because the absorption coefficients are strongly dependent on wavenumber, the pattern observed does not reflect the true abundance of the various OH types. To better evidence the relative importance of the infrared bands appearing in the first hydration step, the first subtracted spectra (spectra b and a in Figure 8E,F) were treated using the proposed relationship relating absorption coefficient to wavenumber[27,28] in silicas: $B = (6462-1.687\nu)^2$. This relation, first established for wavenumbers between 3300 and 3650 cm$^{-1}$, was extrapolated to provide the distribution, $D_{OH}$, of hydroxyl groups between 3760 and 3100 cm$^{-1}$. This was achieved by normalizing the spectra $k(\nu)$ at 3747 cm$^{-1}$: $D_{OH} = k(\nu)B(3747)/(B(\nu))$.[28] The spectra resulting from such a treatment are plotted in Figure 9. It reveals that the first hydration stage is mainly linked to the appearance of two bands at 3653 and 3578 cm$^{-1}$ for Na-magadiite and at 3645 and 3560 cm$^{-1}$ for K-magadiite. As shown in Figure 10, such positions are perfectly coherent with those observed by Raman spectroscopy on Na- and K-magadiites rehydrated during 3 min by

introducing air in a cell previously kept under dynamic vacuum during 15 h, that is, in the first stage of hydration. The combination of Raman and IR spectroscopy in the stretching region thus clearly shows that the 1635 $cm^{-1}$ band can be assigned to weakly H-bonded water molecules. Furthermore, a decomposition of the IR profiles of Figure 9 (not shown) reveals that both components (3650 $cm^{-1}$ with a fwhh of ~70 $cm^{-1}$ and 3570 $cm^{-1}$ with a fwhh of ~120 $cm^{-1}$) have equivalent integrated areas. This confirms that those two bands are related to the same population of water molecules. Then, either these water molecules are bonded to the cations and the two components at 3650 $cm^{-1}$ and 3570 $cm^{-1}$ represent the $\nu_{as}$ and $\nu_s$ modes of water in a $C_{2v}$ symmetry, or only one of the hydroxyl groups (3570 $cm^{-1}$) is weakly H-bonded and the other one is free. The wavenumber of the bending mode at 1635 $cm^{-1}$ clearly favors the second hypothesis. The influence of the nature of the monovalent cation at this stage is marked by a shift toward lower wavenumbers in the case of K-magadiite. Taking into account the observed relationships between $\nu_{OH}$ and the O−O distance in O−H···O bonds,[29] this would tend to suggest shorter O−O distances for K-magadiite. A partial confirmation of such an interpretation can be derived from the evolution of $d(001)$ in this range of relative water vapor pressure. Indeed, K-magadiite exhibits a lower interlayer swelling than Na-magadiite (Figure 6).

For water vapor relative pressures up to 0.04 (Na-magadiite, Figure 8C) and 0.05 (K-magadiite, Figure 8D), very limited changes are noticeable in agreement with other water adsorption results. For higher relative pressures, new components start growing at 3660, 3580, 3430, and 3240 $cm^{-1}$ (Na form) and at 3647, 3580, 3430, and 3230 $cm^{-1}$ (K form). This clearly agrees with the development of a second hydration stage. Even if an unequiivocal assignment of signals in this region cannot be achieved, these positions confirm the interpretation deduced from results obtained in the bending region, that is, water molecules linked to the cations (3660, 3580 $cm^{-1}$) and doubly hydrogen-bonded water molecules (3430, 3240 $cm^{-1}$). Differences between Na- and K-magadiite lie in (i) the higher amount of hydration water found for K-magadiite for high relative pressures in agreement with water gravimetry adsorption results and (ii) the position of the lower frequency component that is shifted toward lower wavenumbers for the K sample. Such a difference could be tentatively assigned to an effect of confinement related to the lower $d$ spacing and higher cation size in potassium-exchanged magadiite.

Figure 11 presents the evolution of the infrared spectra of divalent-exchanged magadiites with increasing water vapor relative pressure. In the $OH_2$ bending region (Figure 11A,B), the infrared signals are rather different from those obtained for Na and K samples because no signal at 1635 $cm^{-1}$ is observed for low relative pressures. However, considering the width of the band centered at 1626 $cm^{-1}$ for Mg-magadiite and its sharpening upon increasing hydration, the presence of a hindered component around 1635 $cm^{-1}$ for low $P/P_0$ values cannot be totally ruled out. With increasing water pressure, the evolution of the spectra for Mg-magadiite is rather similar to what was observed for monovalent samples as the increase of the component at 1626 $cm^{-1}$ is followed by the appearance of a well-defined shoulder at 1665 $cm^{-1}$. The situation is markedly different for Ca-magadiite for which the evolution of the spectra reveals only two signals[30], one at 1625 $cm^{-1}$ at low $P/P_0$ and one at 1645 $cm^{-1}$ that appears for $P/P_0 = 0.15$ and the height of which increases with increasing water content. If, for Mg-magadiite, one believes in the presence of a component around

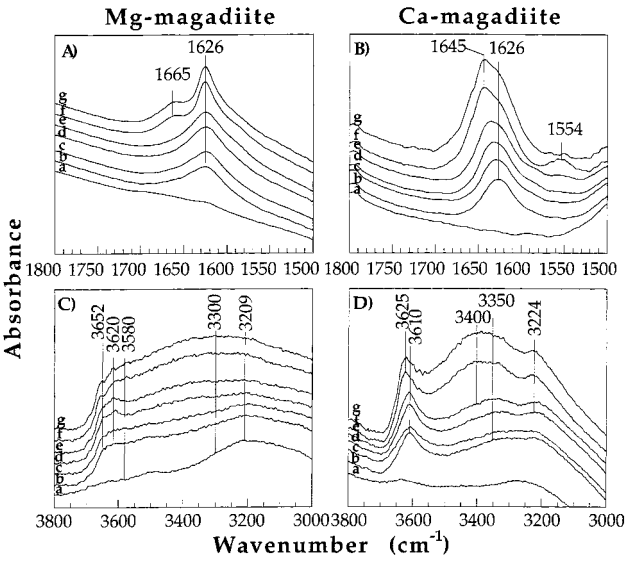


**Figure 11.** Evolution of infrared spectra at 30 °C upon water adsorption of Mg-magadiite (A) and Ca-magadiite (B) in the water bending and in the water stretching (Mg form, C and K form, D) vibration domains. In the case of Mg-magadiite, conditions for spectra a−g were under vacuum and $P/P_0 = 0.018$, 0.050, 0.199, 0.297, 0.594, and 0.860. In the case of Ca-magadiite, conditions for spectra a−g were under vacuum and $P/P_0 = 0.015$, 0.050, 0.150, 0.250, 0.600, and 0.850.

1635 $cm^{-1}$, then the signals observed can be assigned in the same way as previously made for monovalent magadiites, that is, (i) water molecules sharing interactions with both the cation and the silica surface, (ii) water molecules directly linked to the magnesium ion, and (iii) doubly hydrogen-bonded water molecules. However, with regard to monovalent samples, the changes between the different hydration steps are much less clear-cut (no single band at 1635 $cm^{-1}$) and occur at much higher values of water vapor pressure. In the case of Ca-magadiite, the component at 1625 $cm^{-1}$ can be assigned to water molecules interacting with the cation. The position at 1645 $cm^{-1}$ is close to that observed in liquid water. As previously discussed, such a component could also be assigned to water molecules with two nonequivalent OH vibrations. However, because only limited structural changes are associated with the appearance of the component at 1645 $cm^{-1}$, the assignment to liquid water-like molecules would appear more likely. The analysis of the spectra in the OH stretching region should provide a clear answer for assigning the various signals observed for divalent-exchanged magadiite samples.

Unfortunately, spectra obtained in the OH stretching region (Figure 11C,D) are rather noisy with an ill-defined baseline. For this reason, subtractions were not carried out, because they may lead to unreal infrared bands. In the case of the Mg form, it may still be possible to distinguish two main hydration steps. The first one (spectra a−e) is linked to the growth of a signal at 3620 $cm^{-1}$. In this region, when the data are corrected from the variation of absorption coefficients with wavenumber (not shown), it seems that, as in the case of monovalent samples, it may be possible to distinguish a high-frequency and a low-frequency component. This would suggest that water molecules in a $C_1$ symmetry are also present at that stage together with water molecules linked to the $Mg^{2+}$ cation. The second hydration step is related to the appearance of a component around 3652 $cm^{-1}$, coupled with the growth of lower frequency signals (spectra f and g). Two hydration stages can also be observed for Ca-magadiite and can be deduced from the presence of an initial signal around 3610 $cm^{-1}$ (spectra a−e) followed by the

concomitant growth of components at 3625, 3400, and 3225 $cm^{-1}$ (spectra f and g). In that latter case, the observed signals are rather typical of liquidlike water and seem to preclude the existence of water molecules with two nonequivalent OH bonds. The signal at 3625 $cm^{-1}$ may also be assigned to silanol groups the transition momentum of which would change orientation upon hydration, but at that stage of our study no definite conclusion regarding the assignment of that signal can be given.

The results obtained by IR spectroscopy evidence various important points regarding the influence of the nature of the interlayer cation on the hydration of magadiite. Monovalent samples swell in two distinct steps related to clearly distinguishable water statuses. The presence of $Mg^{2+}$ cations in the interlayer space provokes a shift toward higher water vapor relative pressures but with similar spectroscopic signatures though less clearly defined. When $Ca^{2+}$ cations compensate the layer charge, the water statuses associated with swelling are markedly different from all of the other cases, although water adsorption and XRD measurements suggested an equivalent behavior for Ca- and Mg-magadiites. However, the poor quality of the IR spectra for divalent samples prevents a clear understanding of the differences observed between Ca and Mg samples. Additional information regarding those evolutions may be obtained from a detailed vibrational spectroscopic study of the possible modifications of the structural silica framework upon water adsorption. Furthermore, such a study should provide new insights into the cation/water/layer interactions and their role in controlling swelling.

**Structural Role of Water and Cation on the Silica Framework.** *Influence of the Interlayer Cation on the Spectra of Dehydrated Samples.* Figure 12 presents the infrared and Raman spectra of the five ion-exchanged samples obtained under vacuum. Significant differences in the IR spectra can only be observed in the 1000−1200 $cm^{-1}$ range, that is, in the domain corresponding to antisymmetric Si−O−Si stretching modes (TO, LO). H-magadiite and divalent-exchanged magadiite display a much broader massive confirming the $^{29}Si$ MAS NMR results, which revealed a wider distribution of Si−O−Si angles for those three samples when compared to monovalent magadiites. In addition, unassigned bands around 970 and 915 $cm^{-1}$ are present only for the Ca and Mg forms, whereas a component at 876 $cm^{-1}$ exists only in the Ca sample. Additional information can be deduced from the Raman spectra. H-magadiite presents a component at 987 $cm^{-1}$, typical of a Si−OH stretching, whereas the other magadiites exhibit well-defined bands assignable to $Si-O^-$ around 1030−1090 $cm^{-1}$. In this region, Ca-magadiite is markedly distinct because this component is located at 1086 $cm^{-1}$, whereas it is constant around 1080 $cm^{-1}$ for the Na-, K-, and Mg-samples. The particular status of H- and Ca-magadiites is also apparent in the 480−510 $cm^{-1}$ range. Indeed, H-magadiite exhibits a clear band at 487 $cm^{-1}$ assignable to an $O_3$ Si−OH torsional mode,[31] whereas Ca-magadiite displays a component at 510 $cm^{-1}$, which must be assigned to a $Si-O^-$ group[32] strongly perturbed by the presence of Ca atoms in its vicinity. In this range, no bands are visible for Mg- and K-magadiite, whereas a weak shoulder at 497 $cm^{-1}$ can be noticed for both the Na and K sample. Finally, the Raman spectra of the samples under vacuum reveal that the torsional mode of silica tetrahedra evidenced by the 465 $cm^{-1}$ component is not affected by the nature of the exchangeable cation.

*Influence of Hydration Water on the Vibrations of the Silica Framework.* The evolution of the IR spectra of the five ion-exchanged forms of magadiite with water vapor relative pressure is presented in Figure 13. In the case of H-magadiite, in agreement with all of the previously obtained results that confirmed the nonswelling character of this sample, no significant changes are observed on the spectra. The spectra corresponding to the other ion-exchanged forms of magadiites exhibit only very limited changes in the first hydration stage (spectra a−e for divalent samples and a−c for the monovalent ones) because the only noticeable change for all of the magadiites lies in a slight increase of a band around 1230 $cm^{-1}$. For Na-magadiite only, this first hydration step is also accompanied by a decrease of the signal at 704 $cm^{-1}$ and the appearance of a component at 950 $cm^{-1}$. Modifications of the spectra are much more marked in the second hydration stage (spectra f and g for divalent magadiites and d−g for the monovalent ones). Indeed, the signal at 1230 $cm^{-1}$ exhibits a further increase. The band at 780 $cm^{-1}$ grows significantly. The components around 975 and 915 $cm^{-1}$ tend to disappear for Ca- and Mg-magadiite, and in the case of the Ca-sample, this is accompanied by the development of a shoulder around 960 $cm^{-1}$. A band at 948 $cm^{-1}$ appears for K-magadiite, whereas in this region, the spectra for Na-magadiite exhibit a component around 930 $cm^{-1}$. This region must then be assigned to a $\delta$(Si−O−H) influenced by the presence of water molecules.[33] For all samples, the unassigned signal at 780 $cm^{-1}$ is clearly sensitive to water because it exhibits a significant increase in the second hydration stage. Finally in the region around 700 $cm^{-1}$, the signal at 704 $cm^{-1}$ is strongly reduced for Ca- and Mg-magadiite and nearly vanishes for Na-magadiite. K-magadiite displays a similar evolution though the disappearing band is located at 690 $cm^{-1}$.

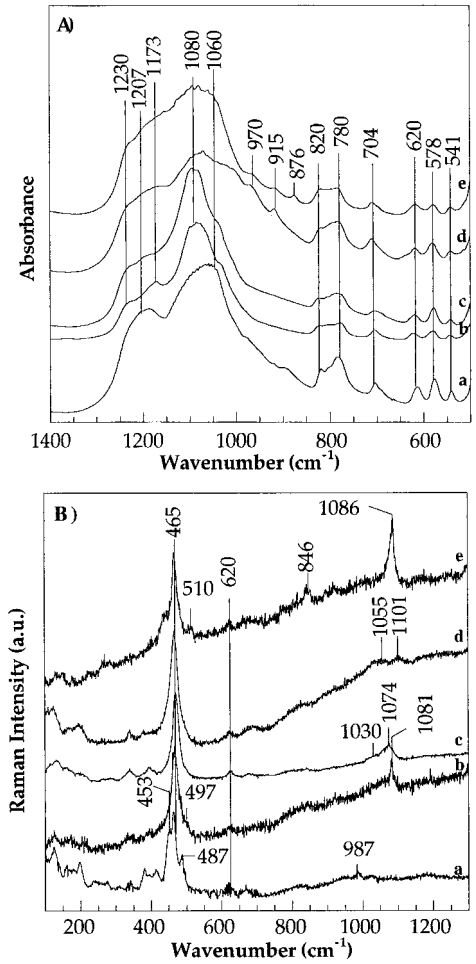


**Figure 12.** Infrared (A) and Raman (B) spectra of the five ion-exchanged magadiites obtained under vacuum: (a) H-magadiite; (b) Na-magadiite; (c) K-magadiite; (d) Mg-magadiite; (e) Ca-magadiite.

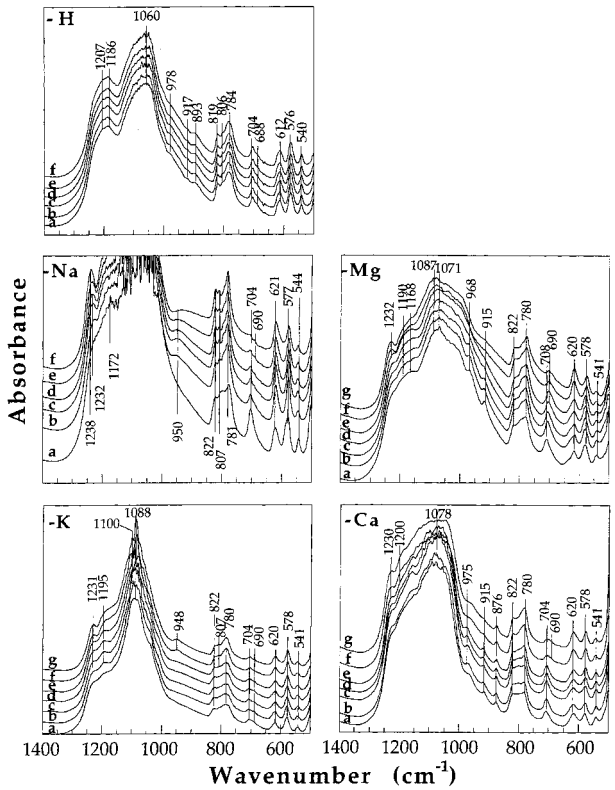


**Figure 13.** Evolution of infrared spectra (1400−500 $cm^{-1}$) of the five ion-exchanged magadiites at 30 °C upon water adsorption. In the case of H-magadiite conditions for spectra a−f were under vacuum and $P/P_0$ = 0.030, 0.063, 0.100, 0.260, and 0.800. In the case of Na-magadiite, conditions for spectra a−f were under vacuum and $P/P_0$ = 0.015, 0.040, 0.060, 0.080, and 0.600. In the case of K-magadiite, conditions for spectra a−g were under vacuum and $P/P_0$ = 0.015, 0.033, 0.050, 0.100, 0.400, and 0.600. In the case of Mg-magadiite, conditions for spectra a−g were under vacuum and $P/P_0$ = 0.018, 0.050, 0.199, 0.297, 0.594, and 0.860. In the case of Ca-magadiite, conditions for spectra a−g were under vacuum and $P/P_0$ = 0.015, 0.050, 0.150, 0.250, 0.600, and 0.850.

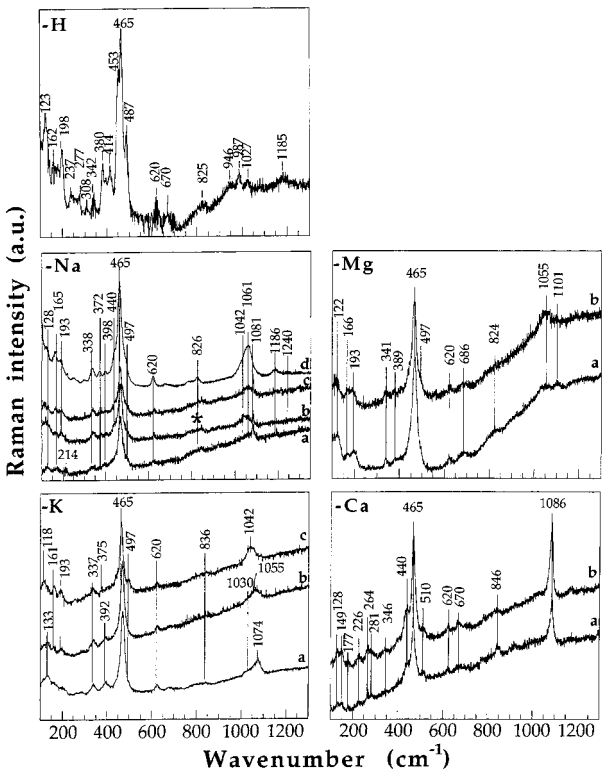


**Figure 14.** Evolution of Raman spectra (100−1300 $cm^{-1}$) of the five ion-exchanged magadiites at 25 °C upon water desorption. In the case of Na-magadiite, conditions for spectra a−d were 0.9 Pa, 40 Pa, 300 Pa, and normal air conditions. In the case of K-magadiite, conditions for spectra a−c were 40 Pa, 100 Pa, and normal air conditions. In the case of Mg- and Ca-magadiite, conditions for spectra a and b were 40 Pa and normal air conditions.

The region around 700 $cm^{-1}$ can be assigned to a $\nu_s$(Si−O−Si) vibration, which appears only when some coupling exists between adjacent silicate layers. When we look at the evolution of IR spectra and take into account XRD results, it appears that this band remains intense for interlayer distances <14 Å, that is, during all of the first hydration step for K-, Mg-, and Ca-magadiites. When the interlayer distance is higher, then the intensity of this signal decreases apparently as a function of the separation between adjacent layers. The lowest intensity of this band at high water vapor relative pressure is indeed observed for Na-magadiite, which presents the highest interlamellar distance.

Raman spectra obtained at various water contents are presented in Figure 14. Compared to infrared data, it is more difficult to derive precise values of water vapor relative pressure for each spectrum. For Ca- and Mg-magadiite, two spectra are presented corresponding to the fully dehydrated state and to a high water content ($P/P_0 \approx 0.5$). For K-magadiite, three spectra are presented corresponding to a partially dehydrated state, a low water content ($P/P_0 \approx 0.05$), and a high water content ($P/P_0 \approx 0.5$). For Na-magadiite, four spectra are presented corresponding to the fully dehydrated state, a low water content ($P/P_0 \approx 0.01$), a medium water content ($P/P_0 \approx 0.1$), and a high water content ($P/P_0 \approx 0.75$). The effect of water content is obvious in different domains of the spectra. In the low-frequency region (<400 $cm^{-1}$), bands around 130, 160, and 200 $cm^{-1}$ increase with water content. In the case of quartz,[34] all low-frequency signals (450, 400, 394, 265, and 128 $cm^{-1}$) assigned to torsional modes of the structure are degenerated. The presence of more components in the case of magadiite suggests that, because of its different structure, the degeneracy is suppressed.

As already mentioned, the torsional mode of silica tetrahedra at 465 $cm^{-1}$ is insensitive to the nature of the interlayer cation. It is also unaffected by water content. The high-frequency side of this component evolves in a similar way for Na-, K-, and Mg-magadiites with the development of a shoulder at 497 $cm^{-1}$. This band is the signature of the formation of Si−$O^-$ and Si−OH groups upon hydration. The fact that it is observed under vacuum for monovalent magadiites is then due to an incomplete dehydration of this sample. In the case of Na-magadiite, this was already suggested by IR spectra in the OH stretching region and must be related to the sample itself. In the case of K-magadiite, it must come from an improper dehydration procedure when recording Raman spectra. In contrast, Ca-magadiite never exhibits this band because the signal at 510 $cm^{-1}$, previously assigned to Si−$O^-$ groups perturbed by the presence of $Ca^{2+}$ ions in their vicinity, remains constant whatever the water content. Related information concerning the layer/water/cation interactions can be found in the region between 1000 and 1100 $cm^{-1}$. Indeed, when dehydrated all of the samples except H-magadiite exhibit sharp signals between 1079 (K-magadiite) and 1101 $cm^{-1}$ (Mg-magadiite). Such signals are associated with the stretching vibrations of the terminal nonbridging oxygens, $\nu$(Si−$O^-$), in $Q^3$ species.[32,34−36] In the particular case of magadiite, they must be associated with a Si−$O^-$−$Ct_{1/z}^{z+}$ association, where Ct stands for an interlayer

cation. For monovalent samples, upon hydration, two new components appear successively at 1042 (Na-magadiite) and 1030 $cm^{-1}$ (K-magadiite), assignable to $Si-O^-(H_2O)-Ct^+$ and 1061 (Na-magadiite) and 1055 $cm^{-1}$ (K-magadiite), assignable to $Si-O^-(H_2O)_x-Ct^+$. For a highly hydrated state, one single band can be observed for both samples. In the case of Na-magadiite, such an evolution is coherent with that observed by $^{29}Si$ NMR CP-MAS measurements carried out on a partially dehydrated sample.[15] Indeed, whereas one single $Q^3$ environment is observed for the hydrated sample (Figure 3), two signals are clearly observed for the partially dehydrated sample, thus confirming the existence of a $Si-O^-(H_2O)-Na^+$ contribution. In the case of Mg-magadiite, one single band appears at 1055 $cm^{-1}$ though the poor quality of the spectrum does not allow fully ruling out the presence of a component around 1040 $cm^{-1}$. In contrast, for Ca-magadiite, this spectral region is totally unaffected, the sharp band at 1086 $cm^{-1}$ being independent of water content. These observations coupled with those made in the spectral region around 500 $cm^{-1}$ definitely confirm the special hydration behavior of Ca-magadiite already suggested from the spectroscopic study of water molecules. The interaction of $Ca^{2+}$ ions with the silica layer evidenced by Raman signals at 510 and 1086 $cm^{-1}$ is strong enough to maintain calcium ions in their inital position when water molecules enter the interlayer space. For all of the other cases studied here, including magnesium, the balance of water/layer/cation interactions enables the displacement of the interlayer cations from their initial position. The peculiar status of calcium likely results from a structural fit between the organization of the silicate layer and the size of the $Ca^{2+}$ species.

## Summary and Conclusions

The information gathered from the combination of thermal analyses, water adsorption gravimetry, and spectroscopic techniques (XRD, NMR, IR, Raman) can be schematically summarized in Figures 15−17, which propose an evolution of the intragallery space of various ion-exchanged forms of magadiite as a function of water content. In all cases, the exact structure and location of water molecules remain partially uncertain because some of these water molecules may be engaged in the creation of silanol groups. Furthermore, the analysis that we carried out is not quantitative because we did not take into account possible preferential orientations of magadiite particles due to their lamellar character. The use of polarized beams would then be needed to address this problem. Additional IR experiments in the near-IR region and the implementation of deuteration procedures would also provide very valuable information for refining the present schematic pictures.

For monovalent cations (Figure 15), the adsorption of the first water molecules displaces the cation from its initial position close to the silicate layer, which generates a water molecule in a $C_1$ symmetry. Once such a displacement is achieved, cation hydration becomes dominant and water molecules are mainly linked to the cation. Finally, some kind of hydrogen-bonded network develops in the interlayer space, but free OH groups appear to be present as well. Such a situation agrees with $^{23}Na$ NMR results[37] that revealed, for hydrated samples, a single environment for sodium ions surrounded by mobile water molecules. Differences between Na-magadiite and K-magadiite being rather limited, it would certainly be fruitful to extend the range of cation polarizablities on both sides by using, for instance, Li- and Cs-exchanged magadiite.

In the case of magadiite exchanged with divalent cations (Figures 16 and 17), the interlayer species could bind either to

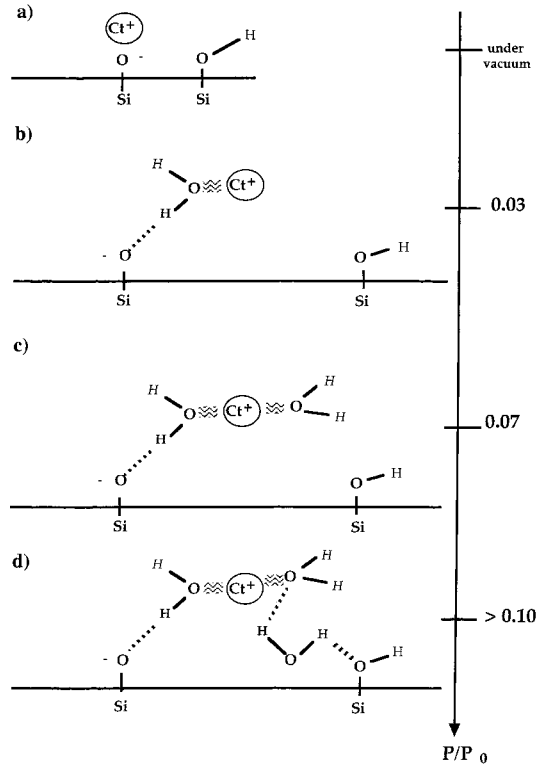


**Figure 15.** Idealized scheme for the different hydration steps of Na- and K-magadiite.

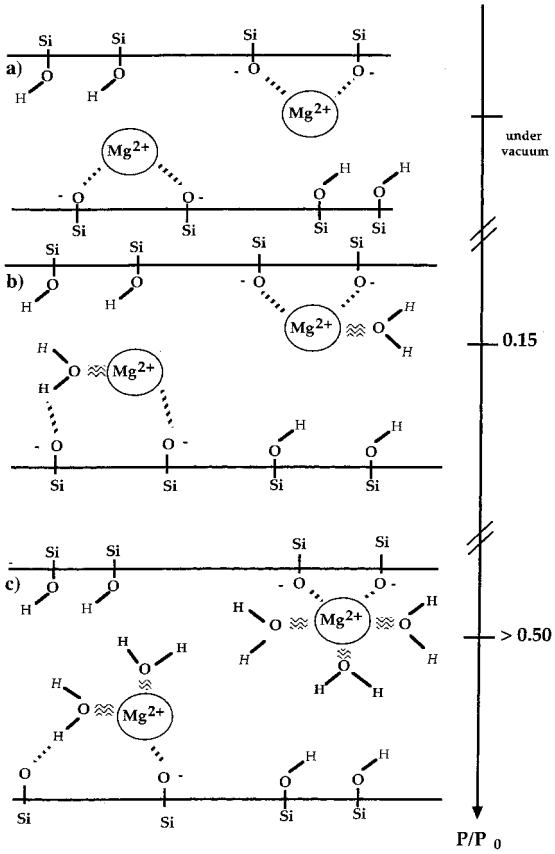


**Figure 16.** Idealized scheme for the different hydration steps of Mg-magadiite.

$SiO^-$ groups belonging to the same clay surface or to $SiO^-$ from two facing sheets. According to the results obtained with $Ca^{2+}$ ions that show that Ca-magadiite swells (Figure 6) while

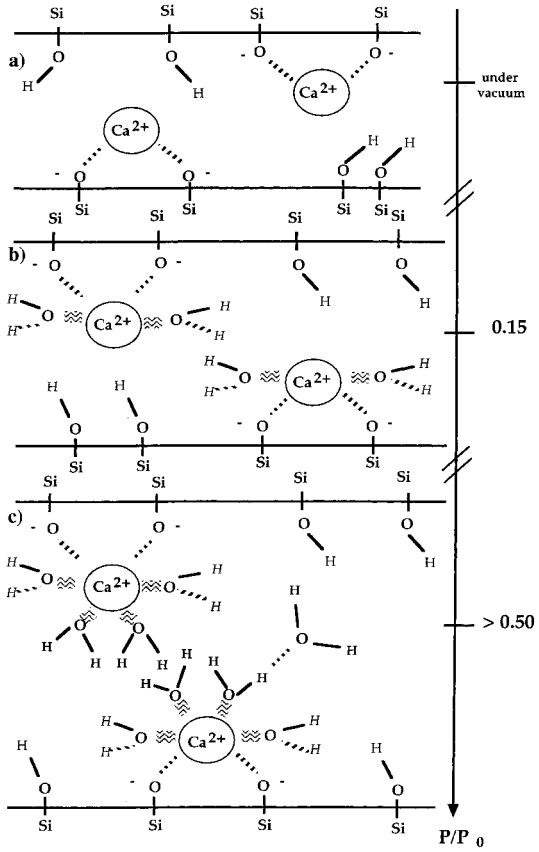


**Figure 17.** Idealized scheme for the different hydration steps of Ca-magadiite.

Si−O−Ca signals at 1086 $cm^{-1}$ remain unaffected by water content (Figure 14), the first situation appears more likely. Depending on the size of the exchangeable cation, different situations are encountered for divalent magadiites. In the case of $Mg^{2+}$ (Figure 16), because of the high polarizability and small size of magnesium, water/cation interactions dominate cation/layer interactions, which displaces magnesium from its initial position. This occurs at much higher relative pressure than in the case of Na- and K-magadiite. Furthermore, even if some water molecules may be in a $C_1$ symmetry, the existence of such a water population does not correspond to a separate hydration step (Figure 16b) but is in a mixed state with water molecules linked to the $Mg^{2+}$ ion. For higher relative pressures, the situation becomes similar to that occurring for Na- and K-magadiites, i.e., a mixture of water molecules linked to the cation, a doubly hydrogen-bonded network, and a few free OH groups. When calcium ions are exchanged in the interlayer space (Figure 17), they interact strongly with $SiO^-$ groups and water/cation interactions are not strong enough for displacing $Ca^{2+}$ from its initial position. For this reason, no water molecules in $C_1$ symmetry develop and only water molecules linked to the cation are observed at first (Figure 17b). For higher relative pressures, liquidlike water molecules are present in the intragallery space but no doubly hydrogen-bonded network develops. In the case of divalent-exchanged magadiite, the balance of interactions then appears to depend on cation size as much as (if not more than) on polarizability. It would then be extremely fruitful to observe the hydration behavior of magadiite exchanged with larger divalent cations such as $Sr^{2+}$ or $Ba^{2+}$.

The general picture arising from our study is that magadiite hydration is markedly distinct from what is observed in other swelling minerals, such as smectites. In the case of aluminum-free layered silicates, cation hydration alone does not explain water adsorption because surface chemistry and surface structure obviously play a major role in structuring water molecules. A better understanding of such phenomena could certainly be achieved by applying the same approach to other minerals of the same family with different charge densities. In that regard, makatite[38] and kanemite[39] of which the crystallographical structures are completely refined would certainly represent very valuable models.

Finally, because vibrational spectroscopies probe very short times only, the image of interlayer water derived from such techniques does not provide any dynamical information in the nanosecond to millisecond range. However, the structural complexity evidenced using vibrational techniques suggests potentially complex dynamics for water and ions in such a confined space, which could be approached using NMR relaxometry and inelastic neutron scattering.

## References and Notes

(1) (a) Farmer, V. C.; Russell, J. D. *Trans. Faraday Soc.* **1971,** *67*, 2737. (b) Prost, R. *Ann. Agron.* **1975**, *26*, 463. (c) Suquet, H.; Prost, R.; Pézerat, R. *Clay Miner.* **1977**, *12*, 113. (d) Cariati, F.; Erre, L.; Micera, G.; Piu, P.; Gessa, C. *Clays Clay Miner.* **1981**, *29*, 157. (e) Sposito, G.; Prost, R. *Chem. Rev.* **1982**, *82*, 553. (f) Bishop, J. L.; Pieters, C. M.; Edwards, J. O. *Clays Clay Miner.* **1994**, *42*, 702. (g) Glaeser, R.; Méring, J. *C. R. Acad. Sci. Sér. D* **1968**, *267*, 463. (h) Bérend, I.; Cases, J. M.; François, M.; Uriot, J. P.; Michot, L.; Masion, A.; Thomas, F. *Clays Clay Miner.* **1995**, *43*, 324. (i) Cases, J. M.; Berend, I.; François, M.; Uriot, J. P.; Michot, L. J.; Thomas, F. *Clays Clay Miner.* **1997**, *45*, 8. (j) Pelletier, M.; de Donato, P.; Thomas, F.; Michot, L. J.; Cases, J. M. In *Clays for our future*; Kodama, H., Mermut, A., Torrance, J., Eds.; 2000; p 555. (k) Slade, P. G.; Quirk, J. P.; Norrish, K. *Clays Clay Miner.* **1991**, *39*, 234. (l) Laird, D. A. *Clays Clay Miner.* **1999**, *47*, 630. (m) Cebula, D. J.; Thomas, R. K.; Middleton, S.; Ottewill, R. H.; White, J. W. *Clays Clay Miner.* **1979**, *27*, 39. (n) Hawkins, R. K.; Egelstaff, P. A. *Clays Clay Miner.* **1980**, *28*, 1. (o) Poinsignon, C.; Estrade-Schwarzckopf, J.; Conard, J.; Dianoux, A. J. In *Proceedings of the International Clay Conference, Denver*; Schultz, L. G., Van Olphen, H., Mumpton, F. A., Eds.; The Clay Minerals Society: 1987. (p) Skipper, N. T.; Soper, A. K.; Smalley, M. V. *J. Phys. Chem.* **1994**, *98*, 942. (q) Skipper, N. T.; Smalley, M. V.; Williams, G. D.; Soper, A. K.; Thompson, C. H. *J. Phys. Chem.* **1995**, *99*, 14201. (r) Powell, D. H.; Tongkhao, K.; Kennedy, S. J.; Slade, P. G. *Clays Clay Miner.* **1997**, *45*, 290. (s) Conard, J. In *Magnetic Resonance in Colloid and Interface Science*; Resing, H. A., Ed.; ACS Symposium Series 34; American Chemical Society: Washington, DC, 1997.

(2) (a) Delville, A. *Langmuir* **1992**, *8*, 1796. (b) Boek, E. S.; Coveney, P. V.; Skipper, N. T. *Langmuir* **1995**, *11*, 4629. (c) Boek, E. S., Coveney, P. V.; Skipper, N. T. *J. Am. Chem. Soc.* **1995**, *117*, 12608. (d) Chang, F. R. C.; Skipper, N. T.; Sposito, G. *Langmuir* **1995**, *11*, 2734. (e) Delville, A. *J. Phys. Chem.* **1995**, *99*, 2033. (f) Young, D. A.; Smith, D. E. *J. Phys. Chem. B* **2000**, *104*, 2033.

(3) Crosnier-Lopez, M. P.; Le Berre, F.; Foirquet, J. L. *J. Mater. Chem.* **2001**, *11*, 1146.

(4) (a) Yun, S. K.; Pinnavaia, T. J. *Chem. Mater.* **1995**, *7*, 348. (b) Wang, J. W.; Kalinichev, A. G.; Kirkpatrick, R. J.; Hou, X. Q. *Chem. Mater.* **2001**, *13*, 145.

(5) (a) Takahara, D.; Kittaka, S.; Kuroda, Y.; Yamagushi, T.; Fujii, H.; Bellissent-Funel, M. C. *Langmuir* **2000**, *16*, 10559. (b) Kittaka, S.; Hamagushi, H.; Shinno, T.; Takenaka, T. *Langmuir* **1996**, *12*, 1078.

(6) Sasaki, T.; Watanabe, M. *J. Am. Chem. Soc.* **1998**, *120*, 4682.

(7) (a) Taylor, H. F. W. *Cement Chemistry*, 2nd ed.; Thomas Telford Edition: London, 1997. (b) Rakiewicz, E. F.; Benesi, A. J.; Grutzeck, M. W.; Kwan, S. *J. Am. Chem. Soc.* **1998**, *120*, 6415. (c) Viallis, H.; Faucon, P.; Petit, J. C.; Nonat, A. *J. Phys. Chem. B* **1999**, *103*, 5212.

(8) Eugster, H. P. *Science* **1967**, *157*, 1177.

(9) McAtee, J. L.; House, R.; Eugster, H. P. *Am. Miner.* **1968**, *53*, 2061.

(10) Brindley, G. W. *Am. Miner.* **1969**, *54*, 1583.

(11) Schwieger, W.; Heidemann, D.; Bergk, K. H. *Rev. Chim. Miner.* **1985**, *22*, 639.

(12) Pinnavaia, T. J.; Johnson, I. D.; Lipsicas, M. *J. Solid State Chem.* **1986**, *63*, 118.

(13) Almond, G. G.; Harris, R. K.; Franklin, K. R. *J. Mater. Chem.* **1997**, *7*, 681.

(14) Eypert-Blaison, C.; Sauzéat, E.; Pelletier, M.; Michot, L. J.; Villiéras, F.; Humbert, B. *Chem. Mater.* **2001**, *13*, 1480.

(15) Eypert-Blaison, C.; Humbert, B.; Michot, L. J.; Pelletier, M.; Sauzéat, E.; Villiéras, F. *Chem. Mater*., in press.
(16) Fletcher, R. A.; Bibby, D. M. *Clays Clay Miner*. **1987**, *35*, 318.
(17) Rojo, J. M.; Ruiz-Hitzky, E.; Sanz, J.; Serratosa, J. M. *Rev. Chim. Miner*. **1983**, *20*, 807.
(18) Rouquerol, J. *J. Therm. Anal*. **1970**, *2*, 123.
(19) Pelletier, M. Thesis, Institut National Polytechnique de Lorraine Nancy, 1999.
(20) Jähnig, R. Diplomarbeit, Universität Leipzig, 1998.
(21) Lagaly, G.; Beneke, K.; Weiss, A. *Am. Miner*. **1975**, *60*, 650.
(22) Rojo, J. M.; Ruiz-Hitzky, E.; Sanz, J. *J. Inorg. Chem*. **1988**, *27*, 2785.
(23) Cases, J. M.; Bérend, I.; Besson, G.; François, M.; Uriot, J. P.; Thomas, F.; Poirier, J. E. *Langmuir* **1992**, *8*, 2730.
(24) Poinsignon, C.; Cases, J. M.; Fripiat, J. J. *J. Phys. Chem.* **1978**, *82*, 1855.
(25) Sposito, G.; Prost, R. *Chem. Rev.* **1982**, *82*, 553.
(26) Franck, H. S. In *Water. A Comprehensive Treatise*. Francks, F., Ed.; Plenum Press: New York, 1972.
(27) Elmer, T. H.; Chapman, I. D.; Nordberg, M. E. *J. Phys. Chem.* **1963**, *67*, 2219.
(28) Legrand, A. P.; Hommel, H.; Tuel, A.; Vidal, A.; Balard, H.; Papirer, E.; Levitz, P.; Czernichowski, M.; Erre, R.; Van Damme, H.; Gallas, J. P.; Hemidy, J. F.; Lavalley, J. C.; Barrès, O.; Burneau, A.; Grillet, Y. *Adv. Colloid Interface Sci*. **1990**, *33*, 91.
(29) Falk, M. In *Chemistry and Physics of Aquaeous Gas Solutions*; Adams W. A., Ed.; Electrothermics and Metallurgy and Industrial Electrolytic Divisions, Electrochemical Society: Princeton, NJ, 1975.
(30) Spectra e−g display a component at 1554 $cm^{-1}$. This band can be assigned to an unidentified organic pollution from the pumping system and not to a water signal. Indeed, deuteration experiments carried out after an adsorption−desorption cycle do not lead to any displacement of this component.
(31) Burneau, A.; Humbert, B.; Barrès, O.; Gallas, J. P.; Lavalley, J. C. In *The Colloid Chemistry of Silica*; Bergna, H. E., Ed.; ACS Advances in Chemistry Series 234; Amercican Chemical Society: Washinton DC, 1994.
(32) Furukawa, T.; Fox, K. E.; White, W. B. *J. Chem. Phys.* **1981**, *75*, 3226.
(33) Burneau, A.; Barrès, O.; Gallas, J. P.; Lavalley, J. C. In *Proceedings of International Workshop on Fourier Transform Spectroscopy*; Vansant, E. F., Ed.; Antwern, Belgium, 1990; p 108.
(34) Bates, J. B. *J. Chem. Phys.* **1972**, *56*, 1910.
(35) Bates, J. B. *J. Chem. Phys.* **1972**, *57*, 4042.
(36) McMillan, P. *Am. Miner*. **1984**, *69*, 622.
(37) Almond, G. G.; Harris, R. K.; Franklin, K. R.; Graham, P. *J. Mater. Chem.* **1996**, *6*, 843.
(38) Annehed, H.; Fälth, L.; Lincoln, F. J. *Z. Kristallogr*. **1982**, *159*, 203.
(39) Garvie, L. A. J.; Devouard, B.; Groy, T. L.; Camara, F.; Buseck, P. R. *Am. Miner*. **1999**, *84*, 1170.